

**EFFECTS OF SELECT PARAMETERS ON ELECTRON  
BEAM WELDING OF AL6061-T6 ALLOY**

**DOC. IV-1243-15**

By

Tom Yost and Stephen Liu

## **ABSTRACT**

Electron beam welding was used for joining Al6061-T6, precision machined, cylindrical sections. The welded assembly exhibited a minimum amount of distortion, but a better understanding of the effects of several key welding parameters on the structural integrity of the weld was required. The contents of this document describe the relative importance and interaction between welding speed, volume of filler, and beam pattern on the microstructural and mechanical properties of the welded joint. Understanding of the relationship between welding parameters and weld properties was accomplished by macrophotography and microstructural examination, microhardness testing, energy dispersive spectroscopy (EDX), and mechanical tensile testing of weld coupons. The results of this study will help quantify the robustness of the EBW process for this common aerospace material and joint geometry and will help determine the impacts of process deviations on weld fidelity in the production environment.

## **ENGINEERING STUDY FLOW**

Electron beam welding is widely considered one of the best welding methods in manufacturing. There are two main reasons for this recognition. One of the reasons is the narrow fusion zone (FZ). When less metal is melted shrinkage is less and distortion is also less. Therefore, precision machined components can be welded together with little or no secondary machining requirements. Another reason is the high efficiency of heat utilization. Not only is there less material melted, but significantly less heat is required to melt it. Hence, the solidification rate can be orders of magnitude greater than arc-deposited weld metal. For comparison, the solidification rate for arc-deposited weld metal is orders of magnitude faster than die casting or permanent mold casting. Solidification for electron beam welded material is associated with fast freezing. [1,2,3]

Al6061-T6 is widely used in the aerospace industry because of its characteristic high strength, good corrosion resistance, high heat conductivity and good low temperature properties. Unfortunately, aluminum alloys with small amounts of magnesium like Al6061 or Al5154 are not suitable for standard arc-welding processes without chemical modifications to the weld pool. Incipient cracking is often observed at the fusion boundary leading to lower mechanical properties.[4] Although not a problem in gas shielded welding, EBW is unique in that it is performed in high vacuum where weld pool modifications are not as simple.

This study investigates the effects of chemical modifications to the weld pool, speed of welding, and beam patterns in the electron beam welding environment on the metallurgical and mechanical properties of Al6061-T6 without the benefit of post-weld heat treatment. The macroscopic, metallurgical, and mechanical analyses were carried out in series as shown in Figure 1.

Note that many of the units provided in this thesis are non-SI units. The U.S. welding industry still uses many of the English and non-standard units. Some dimensions are in inches where typical of the industry. Another example would be the leak rate of  $10^{-4}$  mbar cc/s which corresponds to mbar-l/s in SI units.

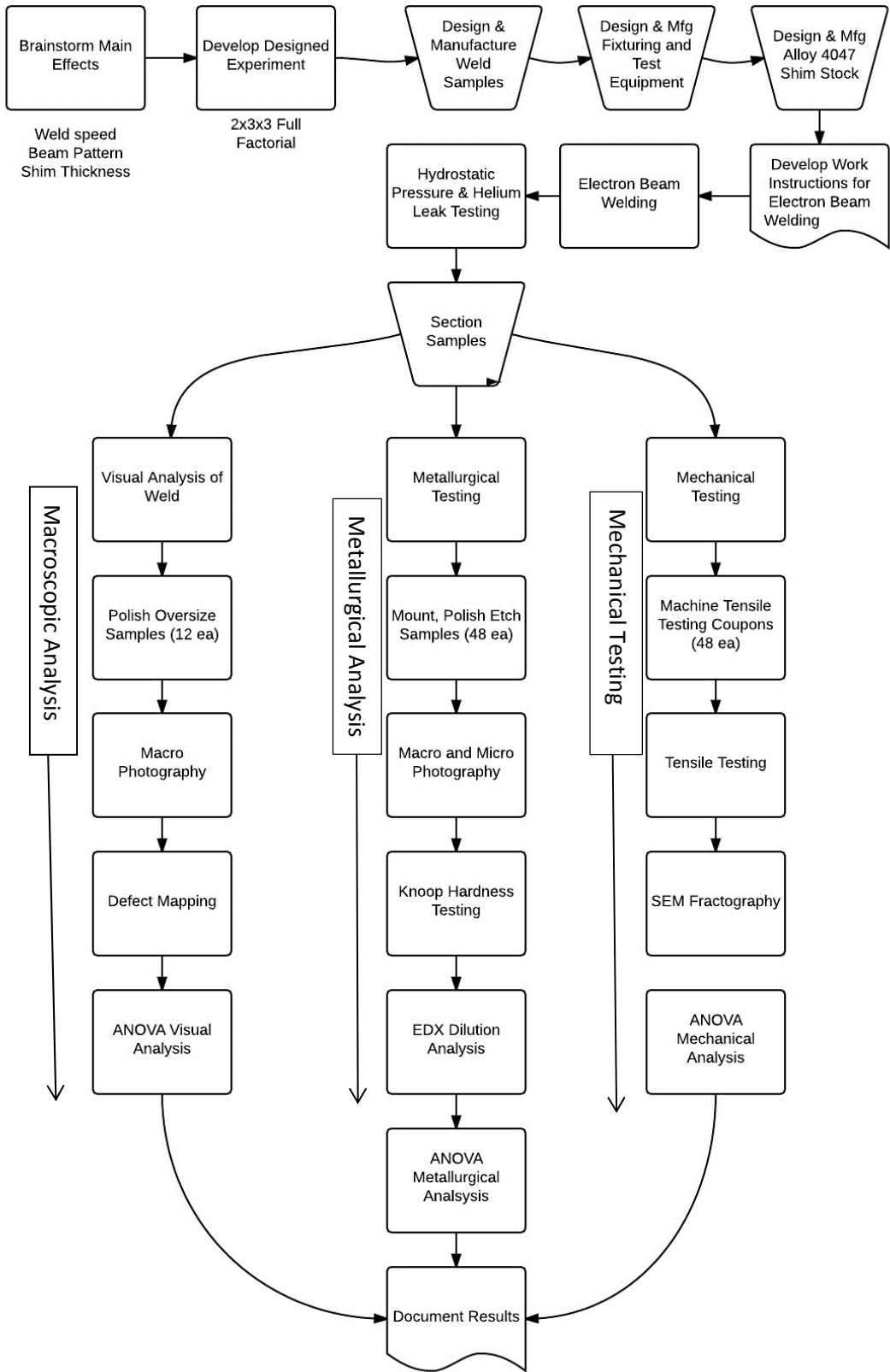


Figure 1 Electron beam welding engineering study flowchart

## ELECTRON BEAM WELDING PRINCIPLES

The invention of electron beam welding can be directly traced to the needs of the nuclear industry. From approximately 1950 onward, there was interest in reactive materials because of their efficiency in capturing neutrons. Selections included niobium, tantalum, zirconium, vanadium, beryllium, molybdenum, tungsten, and their alloys. These were the potential canning materials for the advanced reactors being developed, but without a suitable joining technology none could be used satisfactorily. All of these materials had one property in common; they were all extremely reactive to oxygen and nitrogen at temperatures in excess of 300°C. The impurity levels introduced were high enough to effect the strength and ductility of the metal. For this reason, operations involving welding needed to be conducted in an inert atmosphere. Gas tungsten arc welding (GTAW) shielded with inert gases was initially used with limited success. In 1954, Dr. J.A. Stohr of the French Atomic Energy Commission initiated his developments which led to the publication of his paper in 1957 outlining the use of an electron beam to perform fusion welding in a vacuum.[1,2,3,4]

Modern EBW apparatus involves three main components: the beam generator, the beam manipulation mechanism, and the working chamber. These components may have separate vacuum systems. A schematic representation of an electron beam welding machine is shown in Figure 2.

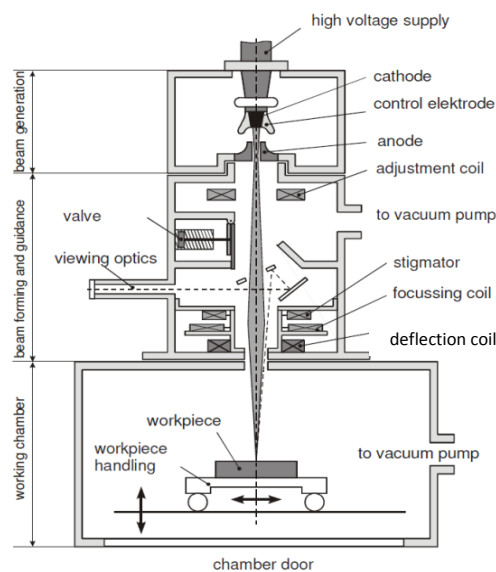


Figure 1 Schematic representation of EBW machine [4]

A tungsten or lanthanum Hexaboride ( $\text{LaB}_6$ ) filament heated to about  $2500^\circ\text{C}$  in a high-vacuum environment ( $10^{-5}$  torrs or lower) will produce free electrons with a current density given by the Richardson-Dushman thermionic emission equation,  $J=AT^2e^{-W/kT}$ . Electrons thermionically emitted from the filament are accelerated by high-voltage towards the anode and a beam of high energy electrons is emitted through the circular hole at its center into the beam manipulation column. The Wehnelt cap, or bias cup, which is positioned between the cathode and anode and is held at a voltage slightly more negative than the filament, regulates the flow of electrons moving through the anode. In principle, the EB generation is identical to the transmission electron microscope (TEM) developed in the late 1930s. Modern TEM and EBW machines use an accelerating voltage of 300kV or more. The EBW gun develops a beam current between 50 to 1000 mA, whereas the TEM employs currents on the order of  $1\mu\text{A}$ , or about  $1/1000^{\text{th}}$  that of the EBW. The electron beam passes through the pierced anode and obtains the power density required to weld. It is then passed through an alignment and focusing system to direct the beam. Several electromagnetic focusing lenses bundle the beam onto the work piece. A stigmator coil helps correct aberrations of the lenses. A viewing optic or video system allows the exact positioning of the EB. The beams typically are focused to about 0.025 to 0.064 centimeters in diameter and have a power density of about  $155\text{K watts/cm}^2$ , which is sufficient to vaporize any metal [1,2,4].

Figure 3 illustrates the EB energy transformation inside the work piece. When the highly accelerated electrons impinge upon the work piece they release their kinetic energy through heat dissipation. Some of the primary electrons are subject to backscatter and secondary electrons along with x-rays.

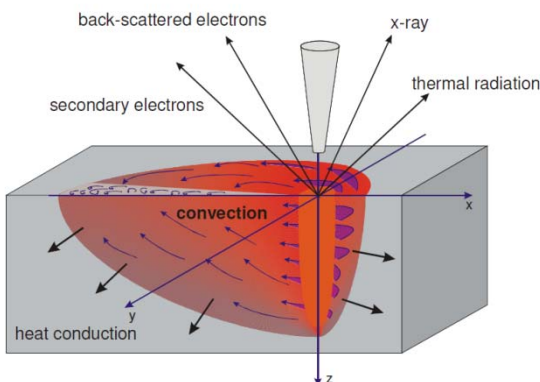


Figure 2 EB energy transformation inside work piece [5]

The impact of the tight beam of electrons only penetrates a few microns into the work piece. The kinetic energy is efficiently imparted to the work piece in the form of heat. The high energy density beam at the point of impact causes the metal to vaporize allowing the formation of a keyhole that is surrounded by a shell of fluid metal for the entire weld depth. As the electron beam advances along the joint, a weld is formed by a combination of three effects that occur at the same time: (1) metal on the advancing side of the hole vaporizes and the vaporized metal then condenses to form molten metal on the trailing side of the hole; (2) the molten metal on the leading side of the hole flows to the trailing side of the hole; and (3) the molten metal formed continuously fills the hole and solidifies as the electron beam advances. Penetration depths of 15 cm in aluminum and 7.5 cm in steel are possible with modern high vacuum, high voltage machines.

## EXPERIMENTAL DESIGN

Table 1 provides the designed experiment factors and their associated levels. The factors included in this research were travel speed, number of metal filler shims, and the EBW beam oscillation. The welding speed was set at 19 and 25 mm/s. This range represented the maximum difference that could be attained without adversely affecting the depth of penetration in practice. The weld dilution was controlled by placing different numbers of 0.0075 mm thick, alloy Al4047 metal filler shims at the joint interface. Zero dilution was represented by no shim material at the joint and the maximum dilution (4 shims) was dictated by the maximum spot size diameter of 0.025 mm. This beam pattern provided a good indication of the effects of beam oscillation on defect reduction.

All other EBW parameters remained constant throughout the testing. The accelerating voltage, beam current, and focus (spot) size were maintained at 60 kV, 19 mA, and 0.025 mm, respectively. The material for the testing was received as extruded Al6061-T6511 tube stock per AMS-QQ-200/8.

Table 1 2X2X3 full factorial DOE factors and associated levels.

Factors	Levels		
Travel speed	19 mm/s	25 mm/s	
Beam Pattern	Straight Beam (no oscillation)	Circular Oscillation (0.25mm)	
Filler Shims	No Shims	2 shims	4 shims

The assembled EBW joint geometry is illustrated in Figure 4. The cylindrical weld joint was machined identical to the final product geometry. The assembly provided a butt joint 6.9 mm thick with an integral backing of 2.5 mm. The integral backing provides a pilot to align the joint and an area for the root of the weld to penetrate that is out of the critical stress zone.

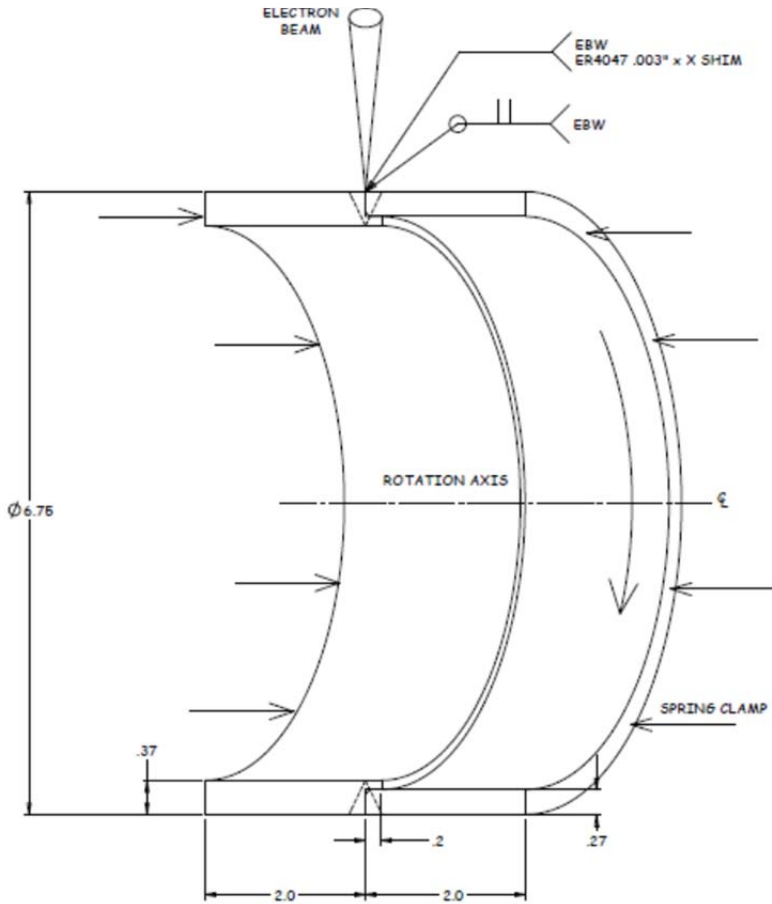


Figure 4 Schematic illustration of welded assembly

Figure 5 shows the fixtured assembly and a representative electron beam weld.



Figure 5 a) weld assembly in fixturing b) weld assembly chucked up inside EB machine c) representative EBW on the outer diameter of welded assembly

Figure 6 illustrates the location and type of weld coupons excised from each weldment. Each of the twelve weldments was cut into four sections, A through D. Each section produced a metallographic and mechanical weld test coupon.

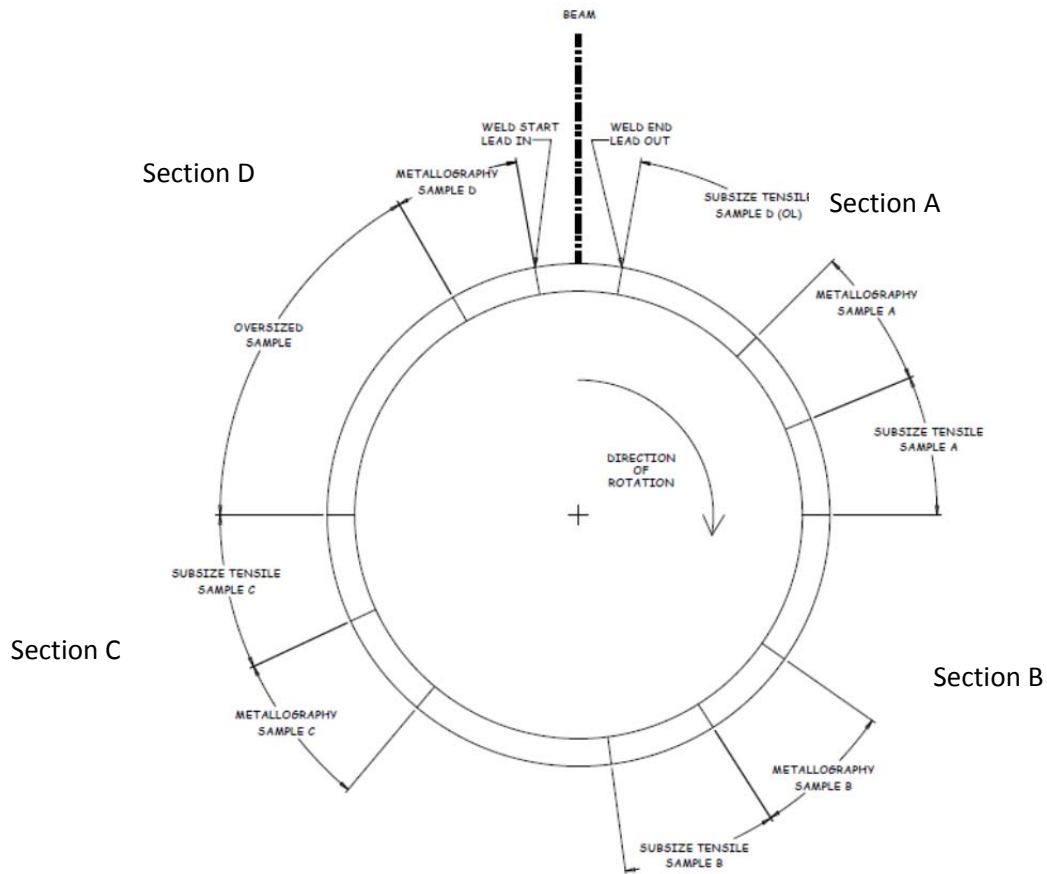


Figure 6 illustrates the tensile sample dimensions and the locations from which they were extracted.

### MACROSCOPIC ANALYSIS OF THE WELD ZONE

A thirty to forty-degree section of each welded assembly was cut out, milled, and polished to create a macrostructural view of the EBW centerline. The oversized longitudinal weld samples were separated into groups for a given main factor. The weld samples were then arranged so that a one to one comparison could be made between tests with identical levels. Visual analysis was used to ascertain the impact of the main factors for all the different levels tested. The arrangements are shown in Figures 7-9.

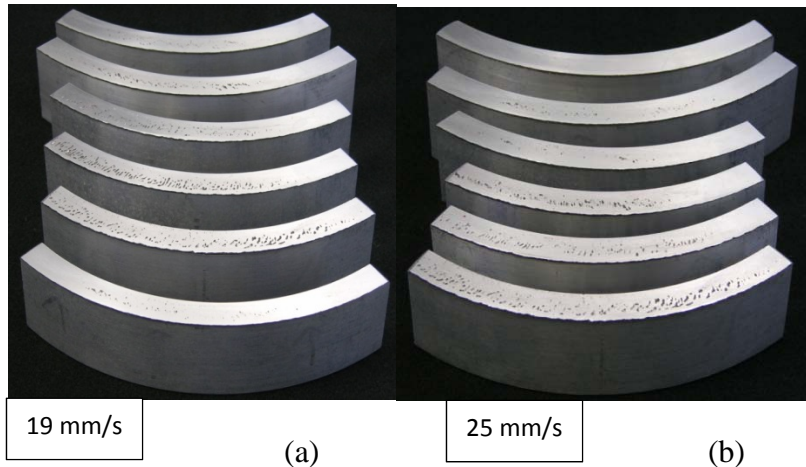


Figure 7 Comparison of defects in longitudinal oversized section welded at different travel speeds: (a) 19 mm/s; (b) 25mm/s

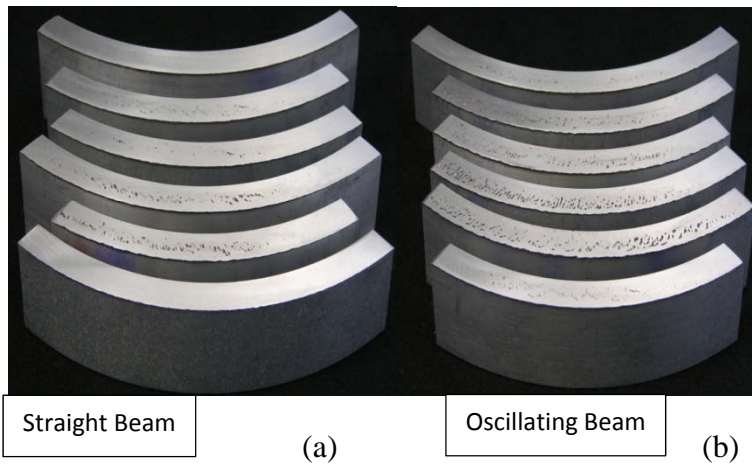


Figure 8 Comparison of defects in longitudinal oversized section welded with different beam patterns: (a) straight beam; (b) oscillating beam

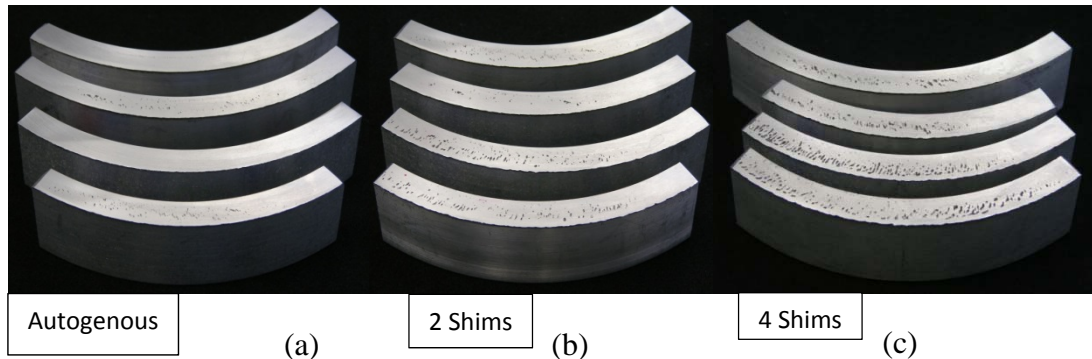


Figure 9 Comparison of defects in oversized longitudinal sections welded with different numbers of shims: (a) no shims; (b) 2 shims; (c) 4 shims

Main effect plots were used to visualize the impact of each welding parameter on the percentage of porosity. Figure 10 shows the main effect plots for this DOE. Factors with steeper slopes had larger effects and provided larger impacts on the results. The travel speed had very little impact on porosity percentage. The beam pattern and shim thickness provided greater impact.

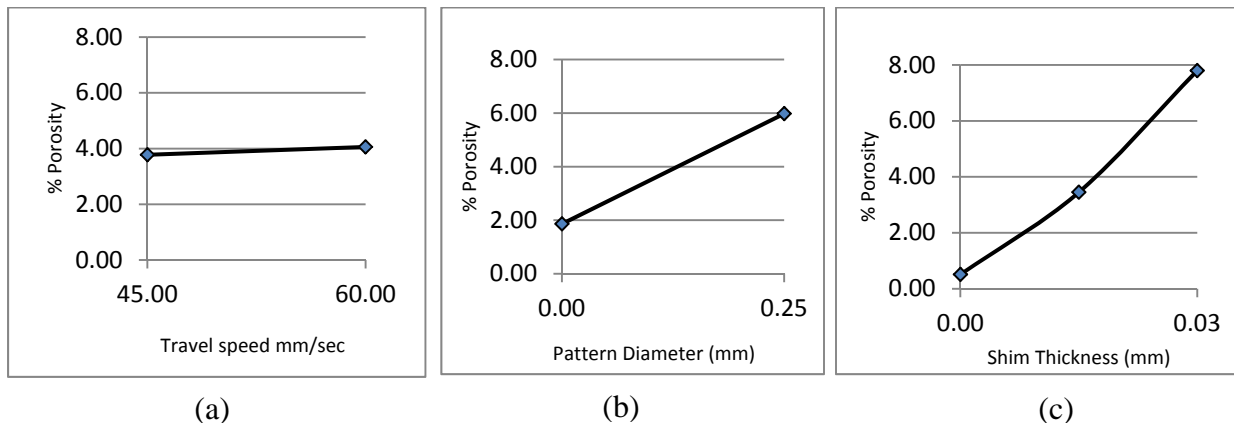


Figure 10 Main effects plots for the percentage of porosity versus select electron beam welding parameters: (a) travel speed; (b) beam pattern diameter; (c) shim thickness

The strong correlation between the shim thickness and defects may mean that the oxide coating was not fully removed before welding. Since the shim thickness was produced by multiple shims of the same thickness (.0075 mm) the number of surfaces with oxide increased by two every time a shim was introduced into the system.

## METALLURGICAL ANALYSIS OF THE WELD ZONE

Figure 11(a) shows optical micrographs of the fusion zones and HAZs in the crown, mid-section, and root of the welds when no Al4047 metal filler shims were used. Centerline solidification cracks were evident in the mid-section and weld root of the autogenous welds. Solidification cracking always occurs in the fusion zone and is mainly due to a lack of molten metal needed to backfill areas being strained by thermal contraction. Liquation cracking was evident in the HAZ of the autogenous welds. Figure 11(b) shows optical micrographs of the fusion and HAZs in the crown, mid-section, and root of the welds when two Al4047 metal filler shims were used. Similar results are present when four shims were placed in the joint. Figure 11(c) shows micrographs of what may be healed liquation cracks in areas of the PMZ when two or four shims were used.

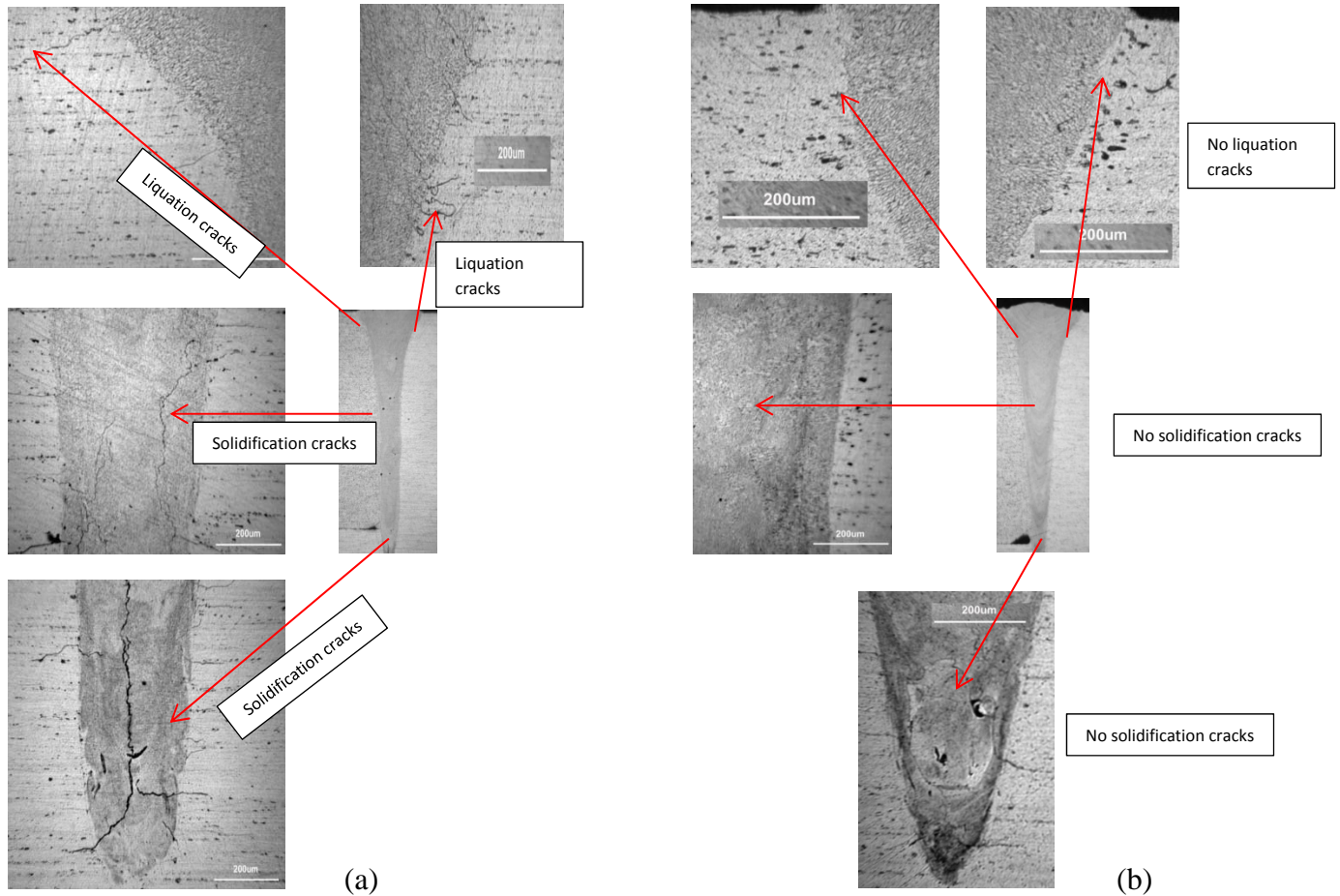
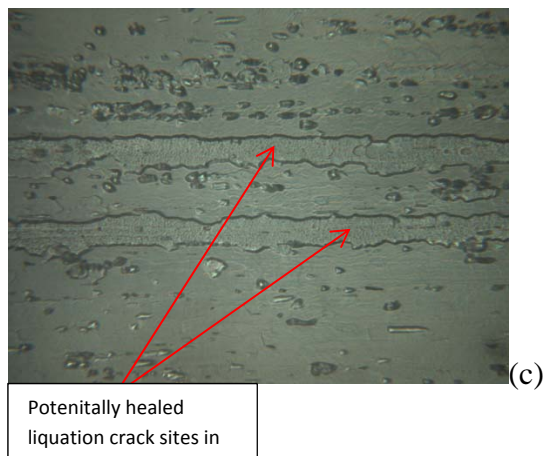


Figure 11 (a) Microstructure showing liquation and solidification cracking in various areas of the weld HAZ and FZ with no metal filler shim. (b) Microstructure showing little or no liquation or solidification cracking with the addition of two Al4047 metal filler shims. (c) High magnification image of area presumed to be healed liquation cracking in the in the HAZ.



OES (Optical Emission Spectrometry) and EDX (Energy Dispersive X-ray) were used to study the dilution effects in the weld zone. Figures 12-14 are bar charts illustrating the dilution of the

Mg and Si in the fusion zone. The horizontal red line indicates the amount of Si required to meet AMS QQ-A-200 for Al6061-T6. The horizontal blue line indicates the amount of Mg required to meet AMS QQ-A-200 for Al6061-T6. The two vertical black lines indicate the EDX measurements taken within the fusion zone. The green dashed line in Figures 3.29 and 3.30 shows the solubility limit of Si in Al in a binary system. Figure 3.28 clearly illustrates the reduction in Si and Mg in the autogenous weld due boiling off in the high vacuum electron beam welding environment.

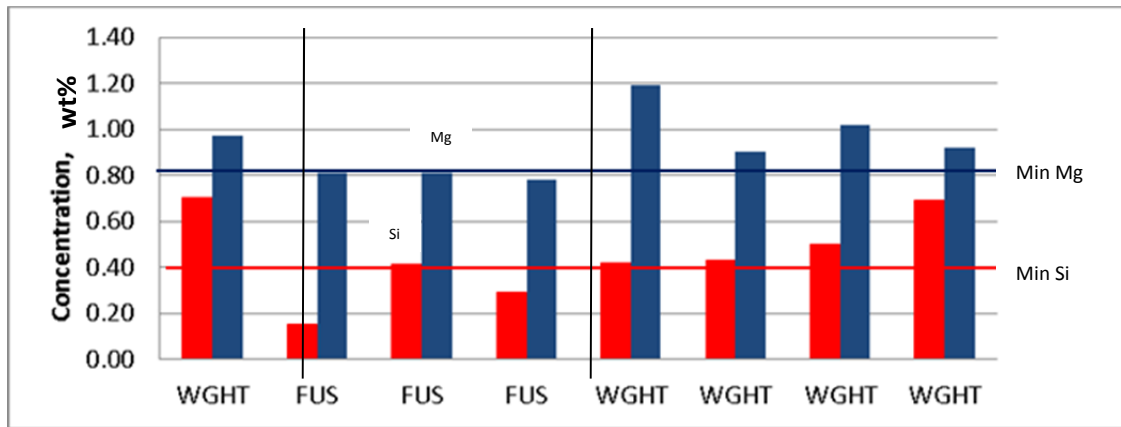


Figure 12 SEI mode x-ray map of Si and Mg dilution for an autogenous weld.

Figure 13 illustrates the large infusion of Si in the fusion zone from the two shims. Since the shim material does not contain Mg its weight percentage continues to decrease due to dilution and boil off. The excess amount of silicon is expected to help heal solidification cracking in the FZ and liquation cracking in the PMZ by forming a eutectic with Al. Although the Mg has been depleted the amount available to produce Mg<sub>2</sub>Si is still adequate for good strength.

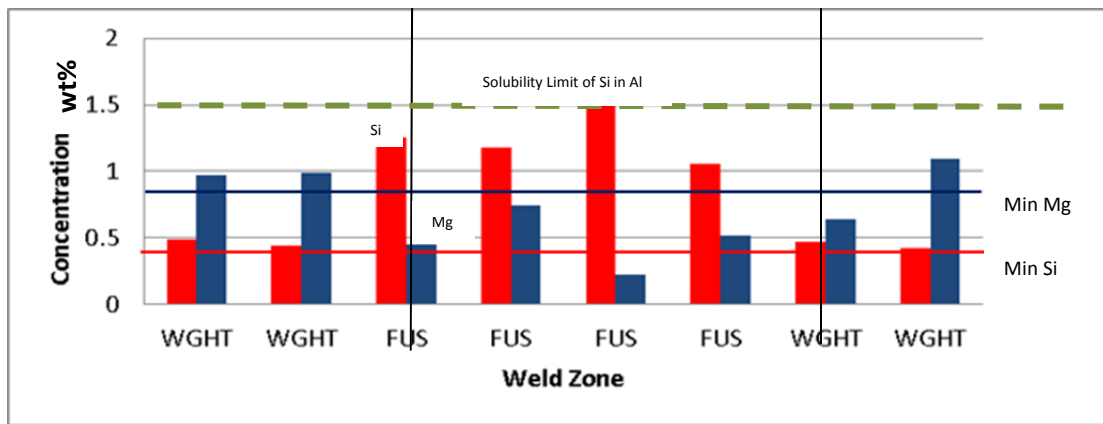


Figure 13 SEI mode x-ray map of Si and Mg dilution with two shims

Figure 14 illustrates the continued infusion of Si and dilution of Mg when four shims are used. The wt. % of Mg is now below the requirements needed to produce an adequate amount of  $Mg_2Si$  for strength. An adequate amount of  $Mg_2Si$  is based upon minimum values of Mg and Si required per AMS-QQ-200/8. The excess Si forms a eutectic with Al and helps to heal hot cracking.

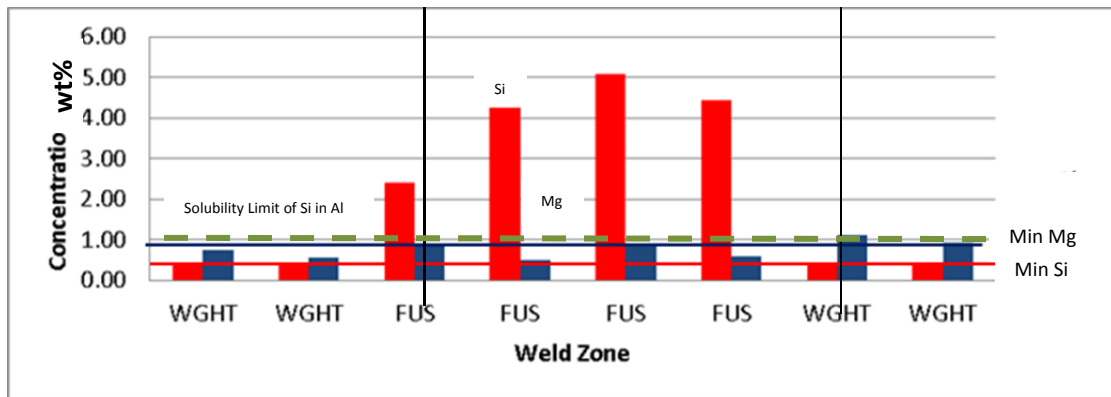


Figure 14 SEI mode x-ray map of Si and Mg dilution with four shims

Table 2 provides the amount of Mg and Si available and used to create the equilibrium phase  $Mg_2Si$  in the fusion zone as a function of the shim count. For example, if 2 shims are used the available amount of Si and Mg is 0.68 wt.% and 1.7 wt.%, respectively. Based on the optimal weight percentage of Mg to Si 1.73:1 only 0.39 wt. % of the Si can be used to create  $Mg_2Si$  ( $0.68:0.39 = 1.73:1$ ). The amount of  $Mg_2Si$  created is the sum of the Mg and Si used, which in this case is 1.1%. This is the minimum amount of  $Mg_2Si$  required to meet the strength requirements for Al 6061-T6 per AMS-QQ-200/8. Excess amounts of Mg and Si stay in solution or precipitate out depending on their concentration. Excess Si is beneficial in the correct amount to backfill solidification cracks in the FZ and liquation cracks in the HAZ.[3] In addition, Table 2 provides the extrapolated equilibrium phase results for the current production process which uses 1 shim. The comments in the table provide insight into the expected outcome based on the amount of alloying elements in the fusion zone.

It is the reduction in Si in the autogenous weld that prevents the required amount of  $Mg_2Si$  from forming. The addition of two shims provides an infusion of Si which helps bring up the amount of  $Mg_2Si$  produced even though the Mg is diluted. The continued dilution of Mg with four shims reduces the amount of  $Mg_2Si$  available for strengthening below the required limits. The

expectation is that the mechanical strength of the autogenous and 4 shim weldments will suffer as a consequence of the lack of  $Mg_2Si$ .

Table 2 Analysis of Mg, Si, and  $Mg_2Si$  in Fusion Zone

	Mg Avail. (wt. %)	Si Avail. (wt. %)	Mg Used (wt. %)	Si Used (wt. %)	$Mg_2Si$ Created (wt. %)	Excess Mg (wt. %)	Excess Si (wt. %)	Comments
0 shims	0.71	0.36	0.62	0.36	0.98	0.09	0.00	$Mg_2Si \rightarrow$ Adequate for strength No excess Si $\rightarrow$ cracking is likely to occur in FZ and HAZ
2 shims	0.68	1.7	0.68	0.39	1.1	0.00	1.3	$Mg_2Si \rightarrow$ Adequate for strength Excess Si $\rightarrow$ Adequate to heal cracks
4 shims	0.50	3.1	0.50	0.29	0.79	0.00	2.8	Low $Mg_2Si \rightarrow$ Not enough precipitate to allow strengthening High excess Si $\rightarrow$ Adequate for cracking.
1 shim	0.70	1.3	0.70	0.40	1.1	0.00	0.90	$Mg_2Si \rightarrow$ Adequate for strength Excess Si $\rightarrow$ cracking is likely to occur in FZ and HAZ

Figure 15 provides the relative crack sensitivities based on the composition of the weld in weight percent of alloying agent. Superimposed on the figure is the  $Mg_2Si$  and excess Si amounts for each of the shim counts for the Al-Mg-Si and Al-Si alloys. The figures show peaks which denote the maximum coherence range for each alloy composition represented. All the welds produced in this study have their  $Mg_2Si$  content at or close to the peak of the Al-Mg<sub>2</sub>Si curve. These welds will incur hot cracking without the help of the liquid Al-Si eutectic. The Al-Si curve shows how the excess Si effects each weld. The autogenous weld has no excess silicon and hence produces little eutectic to prevent hot cracking. The two and four shim welds are off the peak of the Al-Si curve and are expected to provide eutectic to heal hot cracking. The reduction in hot cracking was shown previously in Figures 11. Currently, in production, only one shim is used in the weldments. By extrapolating the data for the autogenous and two shim welds we can estimate the amount of excess Si in the fusion zone of the one shim weld. If the results are correct, the one shim weld is close to the peak for both the Al-Mg<sub>2</sub>Si curve and Al-Si curves indicating a maximized coherency temperature range. The corresponding chemical composition would indicate the current production process may potentially have hot cracking issues.

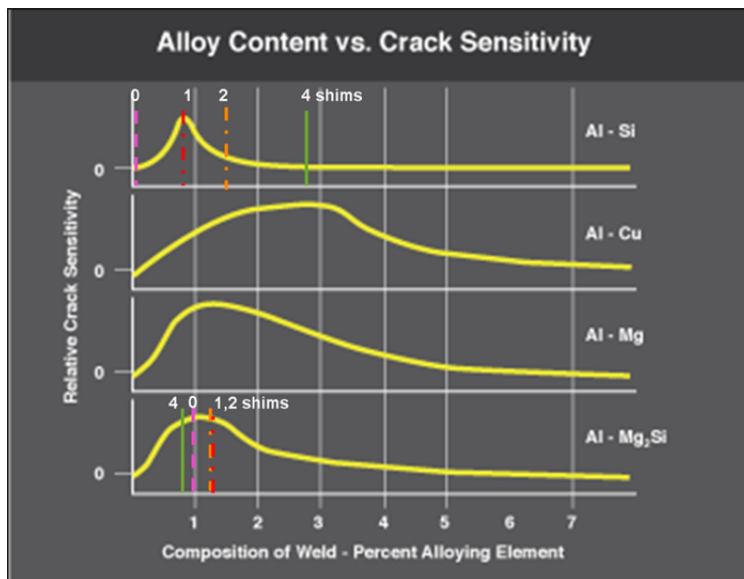


Figure 15 Alloy content versus crack sensitivity for various shim quantities

## MECHANICAL TESTING AND EVALUATION

The mechanical analysis included hydrostatic testing followed by dye penetrant testing, helium leak testing and mechanical tensile testing. All assemblies passed the design requirements set forth on the component drawing. Tensile properties of the EB welded joint were determined by testing conventional flat longitudinal tensile specimens at room temperature. All specimens were tested in the as-welded condition. Table 3 summarizes the averaged metallurgical and mechanical properties of the EB welded joints for the DOE tests performed.

Table 3 Metallurgical and mechanical properties of EB welded joints for DOE tests

Test #	Weld Parameters		Ultimate Strength	Yield Strength	Elongation % *	Fusion Zone Hardness (HK, 100g)	Percent Porosity (%)	Percent change of Si in fusion zone	Percent change of Mg in fusion zone	Joint Efficiency
	Speed mm/s,	Beam Pattern, Thickness mm	MPa	MPa						Ultimate Strength of Joint / Ultimate Strength of Base Metal %
11	19 / STR / 0.000		155.3	149.2	2.9	58	0.0	-75.6	-35.6	50
1	25 / STR / 0.000		159.6	152.3	1.7	68	0.2	-48.0	-12.4	51
12	19 / OSC / 0.000		150.9	143.2	2.0	57	1.2	-74.3	-34.8	49
2	25 / OSC / 0.000		148.5	141.9	1.5	62	1.5	-30.1	-10.8	48
3	19 / STR / 0.015		209.2	194.5	5.8	75	1.9	+60.0	-51.4	67
4	25 / STR / 0.015		219.6	202.7	5.2	73	1.1	+164	-28.1	71
7	19 / OSC / 0.015		198.6	182.6	3.1	75	4.8	+75.0	-38.9	64
8	25 / OSC / 0.015		191.4	180.9	4.2	76	2.7	+194	-16.7	62
5	19 / STR / 0.030		177.9	172.9	2.9	81	3.9	+340	-89.4	57
6	25 / STR / 0.030		189.4	184.2	2.7	80	4.1	+514	-46.3	61
9	19 / OSC / 0.030		154.7	147.2	2.3	79	7.5	+436	-67.9	50
10	25 / OSC / 0.030		166.8	152.9	2.4	83	6.6	+660	-23.9	54

For comparative purposes, Table 4 presents typical mechanical properties for Al6061-T6 and GTAW groove joint welded Al6061-T6 with alloy Al4047 filler wire in the as-welded condition.

Table 4 Mechanical properties of Al6061-T6 and GTAW joints welded with Al4047 filler

Material	Ult. Strength MPa	Yld. Strength MPa	Elongation %
Al6061-T6	310	276	12
GTAW Al6061 with alloy Al4047 filler as-welded	186	124	8

Figure 16 shows the representative engineering stress-strain curves for welds performed autogenously, with two Al4047 shims, and with four Al4047 shims. The loss of ductility for the 2 and 4 shim curves is probably due to the presence of defects. For the zero shim welds there was probably little eutectic liquid due to low Si to back fill the cracks during solidification. In the four shim welds a larger amount of eutectic was expected yet the ductility was low. It is plausible that the low ductility is due to the large number of voids in the fusion zone. The two shim welds had better ductility than either autogenous or the 4 shim welds. They had fewer hot cracks than the autogenous weld and less porosity than the four shim welds. Better ductility could be developed if less porosity was present in the case of the two shim weld. Since bending and impact loading are important design considerations, further study into these types of loads should be considered. Bending loads could be simulated using 3-point bending and the weld toughness by Charpy testing.

In all cases, the specimens fractured in the fusion zone. Tensile results showed significant losses in ductility, owing to strain concentration in the lower strength weld region. Other significant features in a weld that affects ductility is the number of defects, porosity, second phase, or cracks, etc. Gross defects can strongly affect the performance of a weld in tensile testing. Bend and impact testing can better characterize these behaviors.

Weld strength matching can also affect weld mechanical properties. The joint efficiency of the welds in this investigation in terms of elongation never exceeded 5.8% which is not unusual due to the significant strength undermatching encountered in EB welding of age-hardenable aluminum alloys. In undermatching cases, the stress concentration and consequent failure (confined plasticity) generally occur in the lower strength weld region of the joint, leading to an increase of constraint within the weld region, resulting in lower elongation values.

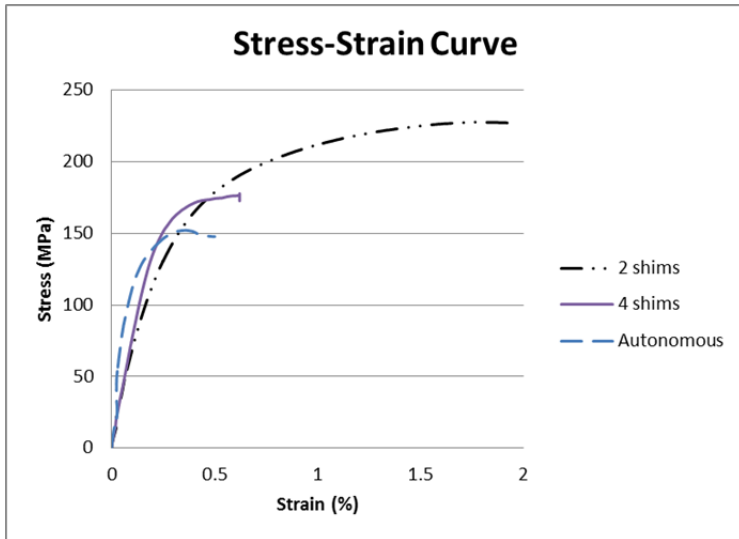


Figure 16 Engineering Stress-Strain curves for EBW performed autogenously and with shims. Strength undermatching could not explain the differences in elongation between the different tests. Dilution testing showed that the autogenous weld had a significant loss of Si and Mg and higher amount of solidification cracking in the fusion zone and liquation cracking in the HAZ. The strength and ductility of the joint were poor. One potential scenario was the remaining Si and Mg combined to form precipitation strengthening  $Mg_2Si$ . The weld became brittle due to the absence of Si required to heal the liquation and solidification cracks. This hypothesis may help to explain the poor mechanical properties when no filler metal was used.

Two shims provided higher strength and better ductility in the joint. The large infusion of Si in the FZ was evident from the percentages measured, although the amount required to reduce weld cracking was not clear. It is likely that one shim may have been sufficient to reduce the liquation and solidification cracking without further diluting the amount of Mg. Two shims introduced the possibility of more surface contamination and more potential for voids that are evident in higher porosity levels. The percentage of porosity may have been a significant factor in the joint efficiency.

Four shims accelerated the detrimental effects experienced with two shims. At this point, cross-sectional area of the shim represents about 2% of the joint volume. This may have been the most significant contributor to the loss of ductility and strength. In addition, since the Al4047 metal filler contains no magnesium its dilution effects became more apparent, and its effects on the strength and ductility of the weld joint become more detrimental.

Increased welding speed reduced element losses slightly, but Mg boil off was still an inherent problem. The straight beam pattern provided a FZ with less porosity than the oscillating beam pattern.

Figures 17-19 illustrate the effects of shim thickness on the mechanical properties of the EB welded joint. The two shim joint has the best overall mechanical properties followed by four shims, and finally the autogenous weld. The poor results for the autogenous weld are based on the lack of excess Si leading to significant solidification and liquation cracking. Four shims produced a large number of voids and diluted the Mg content to the point that there was an inadequate amount of  $Mg_2Si$ , the main strengthening agent in Al, Mg-Si alloys.

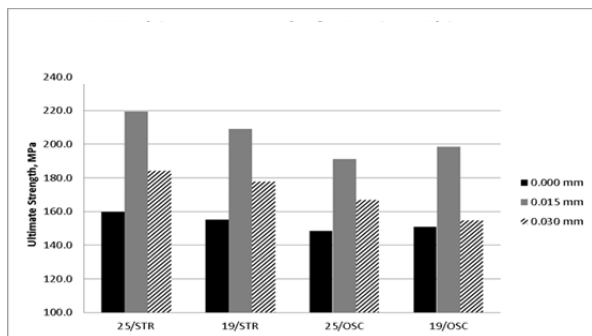


Figure 17 UTS as a function of shim thickness for travel speed and beam pattern

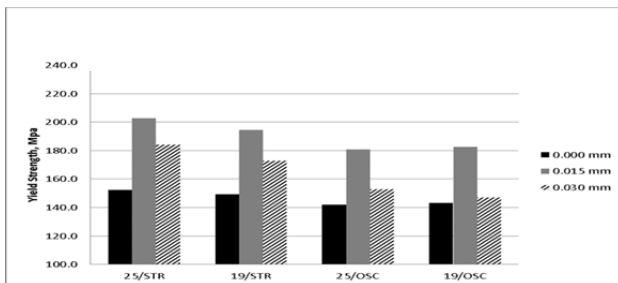


Figure 18 YS as a function of shim thickness for travel speed and beam pattern

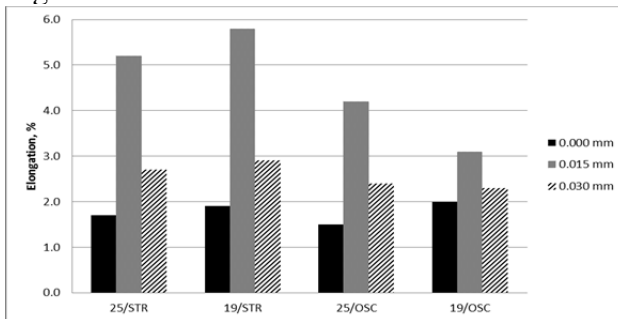


Figure 19 Elongation as a function of shim thickness for travel speed and beam pattern

## CONCLUSIONS

The narrow FZ of the EB weld proved to be extremely sensitive to alloy additions. The autogenous EBW was weak and brittle due to the lack of excess silicon needed for healing solidification cracking in the FZ and liquation cracks in the HAZ. Addition of two filler shims provided increased strength and ductility by reducing solidification cracking, but the improvements were tempered by increased porosity. Four shims proved to be unfavorable for strength and ductility due lack of Mg<sub>2</sub>Si, and further increases in the porosity in the FZ.

The shims provided a consistent infusion of Si to the joint as intended, but the porosity increased dramatically with each addition. Every additional shim provided two more surfaces with gas producing oxides that were trapped in the fusion zone. Further study is needed in understanding the best way to remove oxides and determine the amount of time between oxide removal and welding. Only one shim of the required thickness is recommended in the joint to minimize defects.

The range of travel speeds used in this study did not affect the defects, dilution in the FZ, or mechanical properties of the weld. The speed did affect the weld penetration. Further research is required to understand at what point turbulence in the keyhole column increases the defects in the FZ. Further increases in speed would require an increase in the accelerating voltage to compensate for the decrease in penetration.

The oscillating beam pattern did not provide a reduction in porosity experienced by deep penetration welds in high melt temperature alloys. The oscillating beam pattern produced more porosity, lower strength and less ductility. These observations likely suggests that the benefits seen in deep welds of high-temperature materials may not translate to shallow EBW with low melting temperatures.

Based on the DOE results the best weld parameters for the intended application would be 25 mm/s travel speed, a straight beam and one shim of the correct thickness or chemical composition to provide adequate Mg<sub>2</sub>Si and excess Si. Further research into adequate cleaning procedures are required to remove oxides if shims are to be used.

## REFERENCES

- [1] Funk, R. Edward, “Electron Beam Welding Symposium”, How Metals React to Fusion Welding, (1966).
- [2] Bakish, R., White, S., “Handbook of Electron Beam Welding”, John Wiley & Sons, Inc., New York, (1964).
- [3] Olson D.L. et al, “ASM Handbook: welding, brazing, and soldering, vol. 6.” ASM International, Materials Park, Ohio
- [4] Meleka, A.H., “Electron-beam Welding: Principles and Practice.” McGraw-Hill, 1971
- [5] Dilthey, U., “EB Welding.” ISF Welding Institute, Aachen University (2005) 115-128
- [6] Schubert, G., “EB Welding – Process, Applications and Equipment.”, PTR-Precision Technologies Inc., 120 Post Road, Enfield, CT 06082 USA
- [7] Murphy, Huber, Lever, “Joint Preparation for Electron Beam Welding Thin Aluminum Alloy 5083, “ AWS, April (1990).
- [8] Çam G., Venzke, V., Santos, J.F., Koçak, M. Gonthier-Maurin, Jennequin P., Penasa, M. Rivezla, C., Pract. Metallogr., 37 (2000) 59-89.
- [9] Çam G., Venzke, V., Santos, J.F., Koçak, M. Gonthier-Maurin, Jennequin P., Penasa, M. Rivezla, C., Sci. Technol. Weld. Join 4 (1999)317-323.
- [10] Çam, G., Santos, J.F., Koçak, M., “Laser and EB weldability of Al-alloys.” Literature Review, GKSS 97/E/25, GKSS Research Center, Geesthacht, Germany, 1997, IIW Doc. IX-1896-98
- [11] Martukanitz, Alcoa Laboratories, unpublished research, 1985.
- [12] Lin, D.C., Wang T.S., Srivatsan, T.S. , “A mechanism for the formation of equiaxed grains in welds of Al-Lithium alloy 2090.” Material Science Engineering (2003) 304-309
- [13] Çam, S., and Koçak M. “Microstructural and mechanical characterization of EB welded Al-alloy 7020.” Journal of Material Science (2007) 42:7154-7161.
- [14] Kim, Soosung, Jeong, Yongjin, Park, Jongman, and Lee, Yoonsang. “Fundamental study on EB weld sections and strengths using Al6061-T6 aluminum alloy plate.” Journal of Mechanical Science and Technology (2013) 27: 2935-2940
- [15] Martukanitz R., “Selection and weldability of heat-treatable aluminum alloys, ASM Handbook – Welding, Brazing, and Soldering (1990) 528-536.

- [16] El-Batahgy, A. and Kutsuna, M, “Laser beam welding of AS5052, Al5083 and Al6061 aluminum alloys.”, Advances in Materials Science and Engineering (2009) 1-9
- [17] Allen, C.M., “Laser welding of aluminum alloys – principles and applications.” TWI Report, TWI, Abington, UK, 2004.
- [18] Nair, Biju S., Phanikumar, G., Prasad Roa, K., Sinha, P.P., “Improvement of mechanical properties of gas tungsten arc and EB welded AA2219 alloy.” Science and Technology of Welding and Joining (2007) 579-585
- [19] Ferro, P., Zambon, A., Bonollo, F., “Investigation of electron-beam welding in wrought Inconel 706 – experimental and numerical analysis.” Materials Science and Engineering A392 (2005) 94-105
- [20] Lacki, P., Adamus, K., “Numerical simulation of the EB welding process.” Computers and Structures 89 (2011) 977-985
- [21] Malarvizhi, S., Balasubramanian, V., “Effect of welding processes on AA2219 aluminum alloy joint properties.” Trans. Nonferrous Met. Soc. China 21(2011) 962-973
- [22] Huang, C., Kou, S., “Liquation cracking in full penetration Al-Cu welds.” Welding Journal (2004) 50-58
- [23] Sanderson, A., Taylor, A., “Electron-beam weldability of three aluminum alloys.” Source Book on EB and Laser Welding, American Society for Metals, (1981) 54-59
- [24] Bartle, P.M. “HAZ embrittlement in Al:Zn:Mg alloys”, Select conference on weldable Al-Zn-MG alloys, Welding Institute (1969) 23-25
- [25] Ohsumi, M., Higuchi, K., Hayakawa, Y., Noda, K., “EB Welding of High Strength Aluminum Alloy.”, Source Book on EB and Laser Welding, American Society for Metals, (1981) 60-65
- [26] Adams, C.M., “How Metals React to Fusion Welding.” EB Welding Symposium, Department of Welding Engineering, The Ohio State University Columbus, Ohio, (1966) 27-36
- [27] Stemann, L.G., Seaman, F.D., Goldberg, D.C., “Evaluation of an EB Welding Process for Control Drums.” Westinghouse Electric Corporation Astronuclear Laboratory (1963)
- [28] Arata, Y., Terai, K., Matsuda, S., “ Study on Characteristics of Weld Defect and Its Prevention in EB Welding (Report I).” Trans of JWRI, Vol. 2, No. 1 (1973) 73-112
- [29] Arata, Y., Terai, K., Matsuda, S., “ Study on Characteristics of Weld Defect and Its Prevention in EB Welding (Report II).” Trans of JWRI, Vol. 3, No. 1 (1974) 147-174

- [30] Arata, Y., Terai, K., Matsuda, S., “ Study on Characteristics of Weld Defect and Its Prevention in EB Welding (Report III).” Trans of JWRI, Vol. 3, No. 1 (1974) 174-187
- [31] Arata, Y., “ Super High Energy Density Beam Heat Source and Its Application.” Kinzoku Hyomen Gijutsu, Vol. 24, No 2 (1973)
- [32] Arata, Y., Terai, K., Matsuda, S., Murakami, T., “ Some Dynamic Aspects of Weld Molten Metal in EB Welding.” Trans of JWRI, Vol 2, No 2 (1973)
- [33] Scharuer, D.A., Giedt W.H., Shintaku, S.M., “EB Welding Cavity Temperature Disturbances in Pure Metals and Alloys.” Welding Journal (1978) 127-132
- [34] American Welding Society AWS D1.2, “Structural Welding Code – Aluminum.” (1992)
- [35] Lakshminaraynan, A.K., Balasubramanian, V., Elangovan, K., “Effect of welding processes on tensile properties of AA60601 aluminum alloy joints.” International J. of Advanced Manufacturing Technology (2009) 286-296
- [36] AlcoTec Wire Corporation, “Alloy Al4047 Weld Data Sheet.” 2750 Aero Park Dr., Traverse City, MI 49686-9263, U.S.A (2013)
- [37] Cieslak MJ, Fuerschbach PW, Metall Trans B (1988) 19B: 319.
- [38] Dudas J.H., Collins, F.R., Welding Journal, (1966) 45(6), 241-249.
- [39] G.D. Howden, “An up-to-date look at porosity formation in aluminum weldments,” Welding Journal, vol. 50, no 1, (1971).
- [40] Scott, M.H., Gittos, M.F., “Tensile and toughness properties of Arc-welded 5083 and 6082 aluminum alloys,” Welding Journal vol. 62, no. 9, pp. 243s-252s, 1983.
- [41] Matsuda, F., Nakata K., “Evaluation of ductility characteristics and cracking susceptibility of Al alloys during welding,” Transactions of JWRI, vol. 24, no. 1, (1995) 83-94.
- [42] Woods, R.A., “Porosity and hydrogen absorption in aluminum welds,” Welding Journal, vol. 53, no. 3, (1974).
- [43] Kruger, U., “Beam Welding Processes of Aluminum,” Training in Aluminum Application Technologies, (1994).
- [44] “Metallographic techniques for Aluminum and its Alloys, ”ASM Handbook Volume 9, Metallography and Microstructures of Nonferrous Alloys, (2010)

## **ACKNOWLEDGEMENTS**

With profound gratitude, I thank **Professor Stephen Liu**, Department of Metallurgical and Materials Engineering, Colorado School of Mines for his advice and valuable discussion. It is with pleasure that I thank **Professor Kip Findley and Professor Brajendra Mishra**, Department of Metallurgical and Materials Engineering, Colorado School of Mines for their teaching and insights. I wish to express my thanks to **Gary Frey and Dan Thoren** for their unwavering support of my goals throughout the last three years and the **US Navy** for supporting my thesis work.